Supplementary Information

Unraveling the Electronic Structure and Magnetic Transition Evolution Across Monolayer, Bilayer, and Multilayer Ferromagnetic Fe_3GeTe_2

R. Roemer[†1,2], D. H. D. Lee[†3], S. Smit[1,2], X. Zhang[4], S. Godin[1,2], V. Hamza[2], T. Jian[2], J. Larkin[2], H. Shin[1,2], C. Liu[*1,2], M. Michiardi[1,2], G. Levy[1,2], Z. Zhang[5], R. J. Green[6], C. Kim[7], D. Muller[4], A. Damascelli[1,2], M. J. Han[‡3], and K. Zou[‡1,2]

[1]Department of Physics and Astronomy, University of British Columbia, Vancouver, BC, V6T 1Z1, Canada
[2]Quantum Matter Institute, University of British Columbia, Vancouver, BC, V6T 1Z4, Canada
[3]Department of Physics, KAIST, Daejeon 305-70cc 1, Korea
[4]Applied and Engineering Physics, Cornell University, Ithaca, New York, USA
[5]X-ray Science Division, Advanced Photon Source, Argonne National Laboratory, Lemont, IL, 60439, USA
[6]Department of Physics and Engineering Physics, University of Saskatchewan, Saskatoon, SK, S7N 5E2, Canada
[7]Center for Correlated Electron Systems, Institute for Basic Science and Department of Physics and Astronomy, Seoul National University, Seoul, 08826, Korea
[*]Current Address: Beijing Academy of Quantum Information Sciences, Beijing 100193, China
[†]Equally contributed.
[‡]Corresponding author(s): M. J. Han (mj.han@kaist.ac.kr); K. Zou (kzou@phas.ubc.ca).

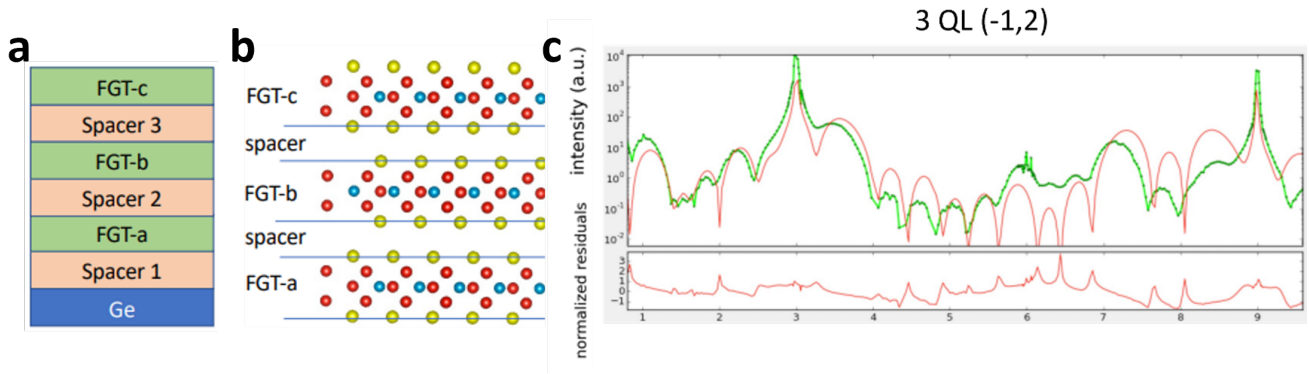

Supplementary Figure 1. Crystal truncation rod (CTR) Characterization of 3 QL FGT Film. a Schematic for the 3 QL sample used for simulating the measured CTR data, including 3 FGT layers and 2 spacer layers. **b** Pictorial representation of the 3 QL structure with atomic positions. **c** CTR data(green) and model (red) of 3 QL along the (-1, 2, L) rod. Here a redefined hexagonal unit cell is used for the Ge (111) surface, with its primary axes [200]h, [020]h, and [003]h defined as [-101]c, [1-10]c, and [111]c in cubic indices, respectively. The simulation/fitting matches with the experimental data fairly well in terms of the oscillation period while the intensities are off at some peaks, likely due to the less-than-perfect coverage in each QL.

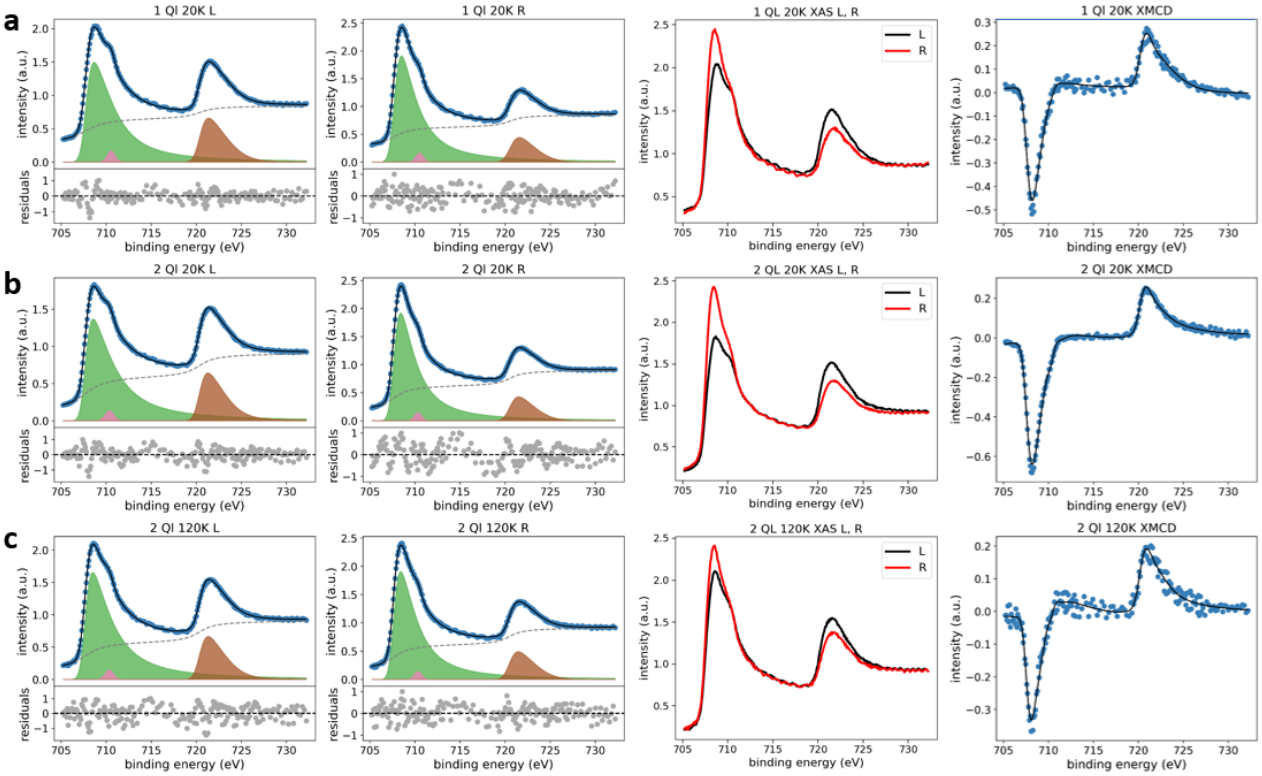

Supplementary Figure 2. Fe L2, L3 edges in XAS and the corresponding XMCD at 20 K and 120 K of 1 and 2 QL FGT films. a, b L2, L3 edges with left and right circularly polarized light, and XMCD results of 1 QL (**a**) and 2 QL (**b**) samples at 20 K. **c** Those with the left and right circularly polarized light and XMCD of 2 QL sample at 120 K (1 QL does not reveal XMCD at this temperature). Our data is well fit using three peaks of Lorentzian and Gaussian line shapes as seen by the small residual. Backgrounds were subtracted using an arctangent background. The structure of the L3 edge does not display many characters, likely due to the covalency and thus strong metalicity in agreement with bulk samples[1]. L3 peaks were fit with two peaks. Although two peaks were identified in the L2 edge, only one peak displayed adequate intensity in our fits. The third panel shows XAS the intensity for both left and right circular polarizations illustrating the differences in absorption that give rise to the magnetic dichroism signal plotted in the subsequent column. No peak position shift is observed with temperature variation. In the 2 QL sample, increasing temperature increases the L3 edge intensity and a softening of the shoulder peak. In the L2 edge, the opposite trend is observed. No such trends are observed in the 1 QL sample. In our course temperature probes, XMCD is retained for 1 QL samples at 20 K and is absent at 120 K. In 2 QL samples, the XMCD disappears between 120 K and 200 K.

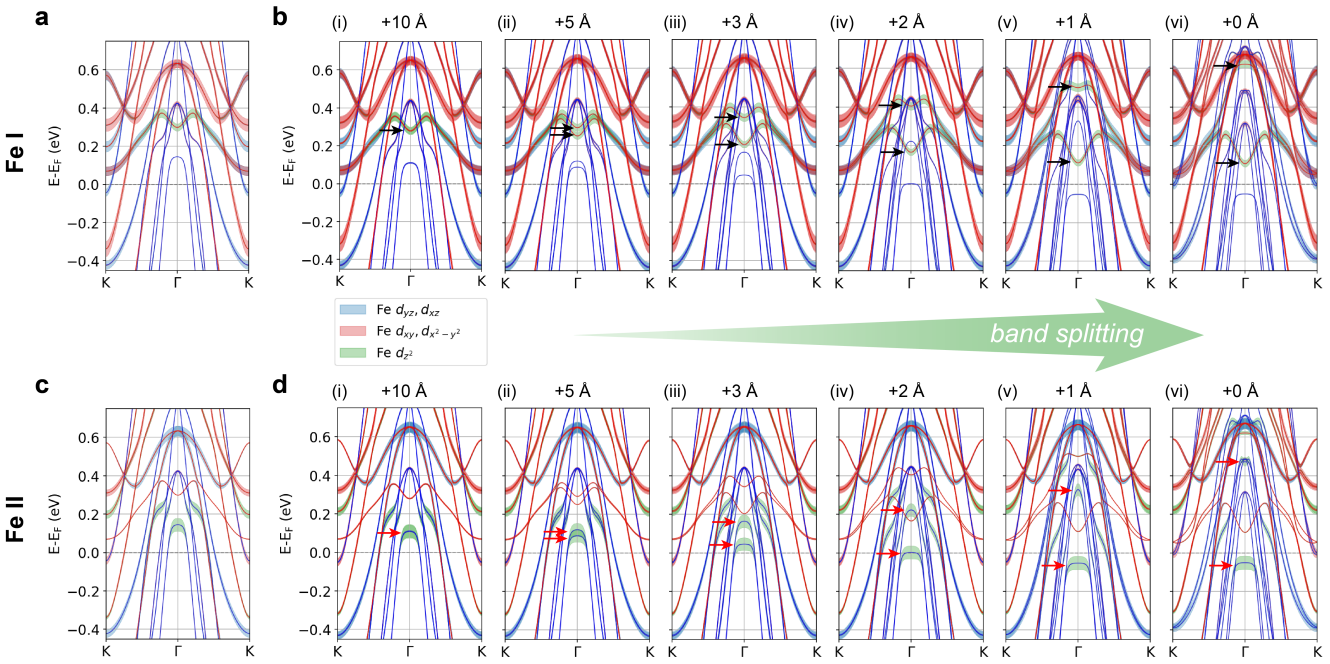

Supplementary Figure 3. Band splitting in 2 QL due to the interlayer coupling. The calculated band structures projected on the Fe I (**a**, **b**) and Fe II (**c**, **d**) sites. **a**, **c** 1 QL band structure as a reference. **b**, **d** The evolution of 2 QL band structure with decreasing interlayer distance of 2 QL. The deviations from its equilibrium value of 8.23 Å (set as +0 Å) are denoted at the top of each subplot (i)–(vi). When the interlayer distance of 2 QL is 10 Å larger than its equilibrium value, the band structure of 2 QL becomes essentially indistinguishable from that of 1 QL. As the interlayer distance approaches its equilibrium value, clear bands splitting near Γ with Fe II (Fe I) d_{z^2} character occurs, as denoted by red (black) arrows in **d** (**b**). Blue and red solid lines represent spin-up and spin-down bands, respectively.

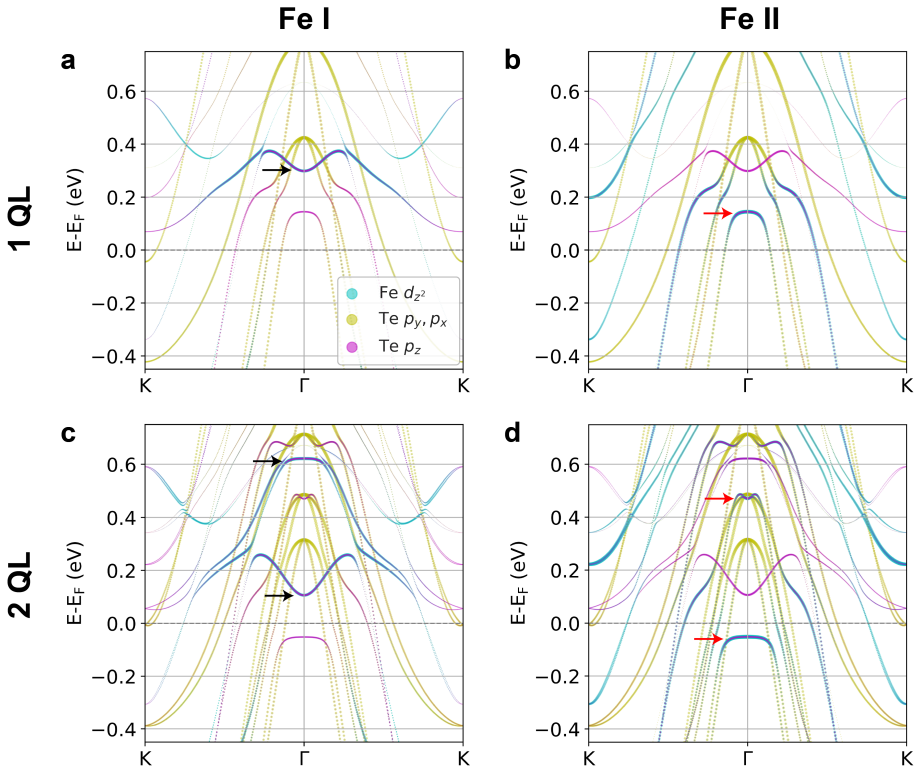

Supplementary Figure 4. Orbital hybridization and interlayer coupling. The orbital-projected band structures of 1 QL (**a**, **b**) and 2 QL (**c**, **d**). The cyan, yellow, and magenta colors represent the Fe d_{z^2}, Te p_x/p_y, and Te p_z characters, respectively, and the circle size shows the relative portion of the orbital characters. The Fe d_{z^2} character is projected on the Fe I (**a**, **c**) and Fe II sites (**b**, **d**). The black (in **a**, **c**) and red (in **b**, **d**) arrows denote the splitting of Fe I and Fe II d_{z^2} bands near Γ as thickness increases from 1 QL to 2 QL, respectively. Note that the bands showing strong hybridization between Fe d_{z^2} and Te p_z exhibit substantial splitting in 2 QL, indicating that the hybridization with Te p_z orbital plays an important role in the interlayer coupling.

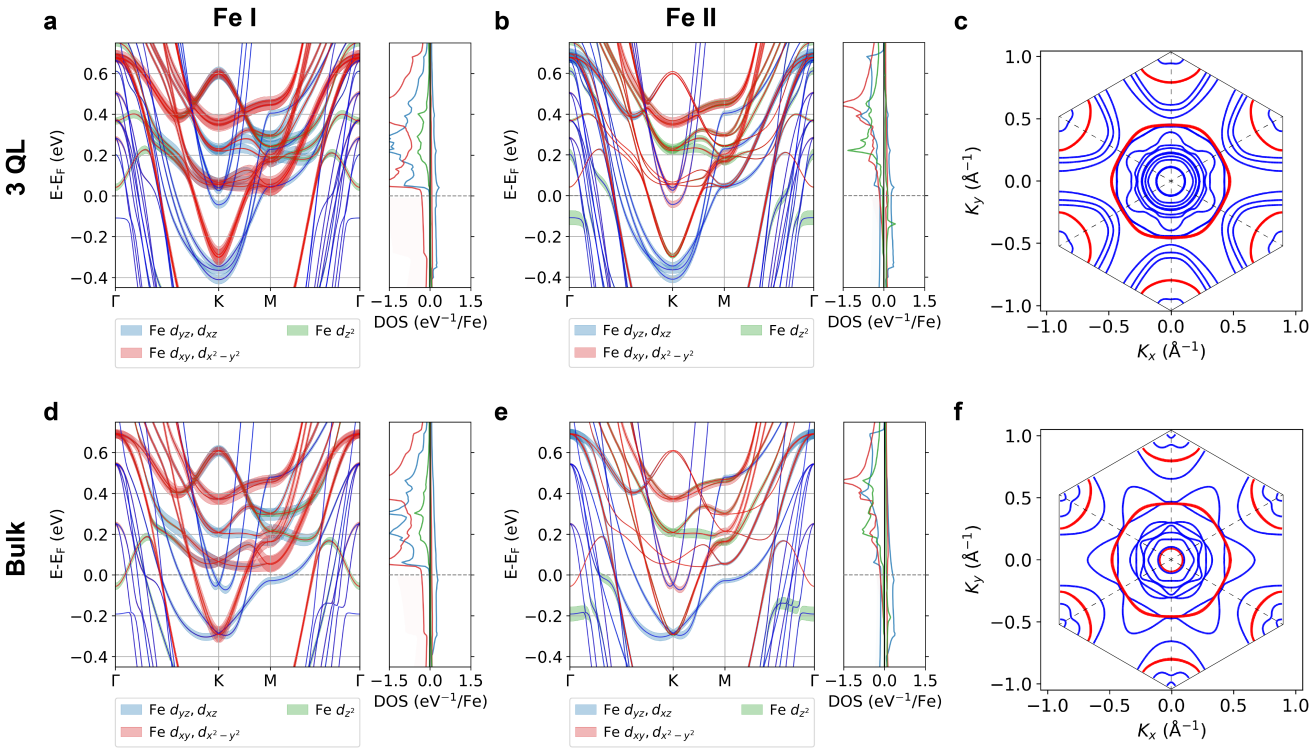

Supplementary Figure 5. Site-spin- and orbital resolved DFT band structure for 3 QL and bulk. Calculated band structures along high symmetry cuts and corresponding projected density of states (DOS) per Fe atom for 3 QL (**a**, **b**) and bulk (**d**, **e**). The projection onto the Fe I (**a**, **d**) and Fe II (**b**, **e**) 3*d* orbitals are also shown. **c, f** Calculated Fermi surfaces at $k_z = 0$ plane for 3QL (**c**) and bulk (**f**). The spin-majority and minority bands are plotted in blue and red lines, respectively.

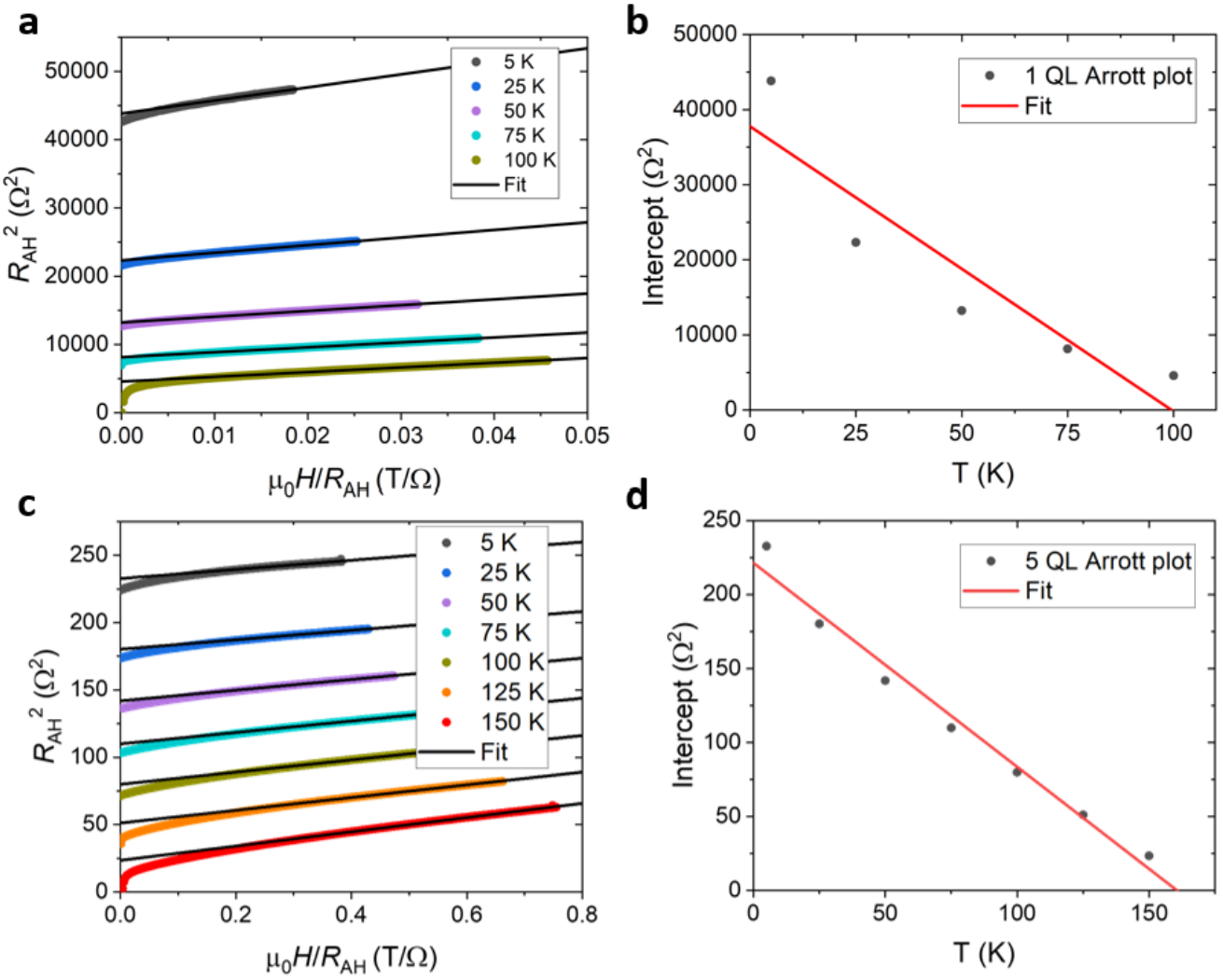

Supplementary Figure 6. Arrott plot analysis of 1 and 5 QL FGT. a(**c**) 1 (5) QL Antisymmetrized R_{xy}^2 plotted against $\mu_0 H/R_{xy}$. The saturated, high-field region of the data is linearly fit and overlaid. **b**(**d**) The y-intercepts of the fits in **a,c** plotted at their respective temperatures. The intercepts are linearly fitted and the x-intercepts of the fit determine T_C in accordance with Deng. et al[2]. Deviations from linearity are used to determine the error bars in the estimation of T_C in **Fig. 3b** of the main text. This sample yields a T_C of 99.58 K $\pm$ 26.8 K (160.69 K $\pm$ 11.65 K).

References

1. Park, S. Y. *et al.* Controlling the Magnetic Anisotropy of the van der Waals Ferromagnet Fe_3GeTe_2 through Hole Doping. *Nano Lett.* DOI: 10.1021/acs.nanolett.9b03316 (2019).

2. Deng, Y. *et al.* Gate-tunable room-temperature ferromagnetism in two-dimensional Fe_3GeTe_2. *Nature* **563**, 94–99, DOI: 10.1038/s41586-018-0626-9 (2018).